Laser spectroscopy of Na I quartets

D. E. Holmgren, D. J. Walker, D. A. King, and S. E. Harris
Edward L. Ginzton Laboratory, Stanford University, Stanford, California 94305
(Received 24 September 1984)

By using a pulsed hollow-cathode discharge, metastable atoms are produced in the $(2p^5 3s\,3p)^4D_{7/2}$ and $(2p^5 3s\,3p)^4S_{3/2}$ levels of Na I. A tunable laser is used to excite these atoms to levels in the $2p^5 3s\,3d$ and $2p^5 3s\,4s$ configurations, and thereby to establish a partial Grotrian diagram for the quartet system. Several possible Na I xuv laser systems are described.

I. INTRODUCTION

Because of their metastability against autoionization, the core-excited quartet levels of alkali-metal atoms and alkali-like metal-ions are of interest for the construction of xuv lasers[1,2] and for studies of atomic and molecular collisional phenomena. In this paper we report the results of a set of experiments in which a pulsed hollow-cathode discharge is used to produce metastable atoms in the $(2p^5 3s\,3p)^4D_{7/2}$ and $(2p^5 3s\,3p)^4S_{3/2}$ levels of Na I. A tunable laser is used to excite these atoms to levels in the $2p^5 3s\,3d$ and $2p^5 3s\,4s$ configurations. The observed enhanced fluorescence, together with Hartree-Fock calculations using the atomic-physics code RCN/RCG,[3] allows the identification of 15 levels and 30 transitions within the quartet manifold.

The quartet levels of Na were first discussed by Feldman and Novick in 1967.[4] More recent studies have used optical absorption from the Na ground level[5] and from the first excited level[6] to identify several core-excited levels. Identifications based on ejected-electron spectroscopy[7] and on xuv emission spectroscopy[8,9] have also been described. Higher wavelength resolution is obtained by working with visible transitions within the quartet manifold. Based on theoretical work by Weiss, the transition $(2p^5 3s\,3p)^4D_{7/2} \rightarrow (2p^5 3s\,3d)^4F_{9/2}$ at 3882 Å was reported by Berry *et al.*[10] Recently Fröhling and Andrä[11] identified the transition $(2p^5 3s\,3p)^4D_{7/2} \rightarrow (2p^5 3s\,4s)^4P_{5/2}$ at 5071 Å.

Section II of this paper discusses the selection rules which bear on the metastability of the Na quartets. Sections III and IV describe the experiments and give the results of this work. Section V describes the parameters of several possible xuv lasers, and Sec. VI summarizes the paper. The Appendix gives details of the calculations using the atomic-physics code RCN/RCG.

II. METASTABILITY AND QUASIMETASTABILITY

In very light alkali-metal systems (for example, Li), where L and S are good quantum numbers, all quartet levels which lie below the first excited ionic level are quite metastable against autoionization. Doublet levels with odd angular momentum and even parity, or even angular momentum and odd parity, are also forbidden to autoionize.

In heavy alkali-metal systems (for example, Cs), there are two classes of atoms which are usually metastable against autoionization. First are those quartets which have the maximum allowable J within a given configuration. To the extent that configuration mixing is not important, these levels are pure quartets and may not autoionize Coulombically.

A second class of levels which, even in heavier atoms, autoionize slowly has recently been termed quasimetastable.[12] Considered in a LS basis, these levels are of mostly quartet character, but are mixed partially with doublets by the spin-orbit interaction. Selection rules for $L\cdot S$ matrix elements, however, only allow them to couple in first order to those doublet levels which themselves are prohibited from autoionizing. The selection rule[12] for these quasimetastable quartets is summarized by the requirement that parity and orbital angular momentum be both even or both odd, and that $|J-L|=\frac{3}{2}$. Because these quasimetastable levels couple to radiating doublet levels, they may be observed by xuv emission spectroscopy.

In Na the lowest configurations of the quartet manifold are $2p^5 3s\,3p$, $2p^5 3s\,3d$, and $2p^5 3s\,4s$. Spin-orbit coupling causes substantial mixing of doublet and quartet levels. As a result, with the exception of the metastable and quasimetastable levels, the calculated autoionizing rates of most doublet and quartet levels are between 10^8 and 10^{10} sec^{-1}.

The lowest level of the quartet manifold is the quasimetastable level $(2p^5 3s\,3p)^4S_{3/2}$. Based upon the photoabsorption measurements of Sugar *et al.*[6] and the work to be described in later sections of this paper, the energy of this level relative to the Na ground level is 263773 ± 15 cm^{-1}. Neglecting configuration interaction, its calculated composition (RCN/RCG) in a LS basis is

$$|{}^4S_{3/2}\rangle = 0.98\,|{}^4S_{3/2}\rangle - 0.15\,|{}^4P_{3/2}|\,\rangle$$
$$+0.07\,|({}^1P)^2P_{3/2}\rangle + 0.04\,|({}^3P)^2P_{3/2}\rangle$$
$$-0.001\,|({}^1P)^2D_{3/2}\rangle - 0.001\,|({}^3P)^2D_{3/2}\rangle\ .$$

The (0.07) and (0.04) components of $({}^1P)^2P_{3/2}$ and $({}^3P)^2P_{3/2}$ result in a calculated xuv radiative rate at 405.2 Å of 7.7×10^6 sec^{-1}. The (0.001) components of $({}^1P)^2D_{3/2}$ and $({}^3P)^2D_{3/2}$ lead to a calculated autoionizing rate of 6.1×10^5 sec^{-1}. When nearby configurations are included to interact with $2p^5 3s\,3p$ in these calculations,

TABLE I. Relative term energies, designations, and Coulombic autoionizing rates of Na I core-excited quartet levels.

Configuration	Energy (cm^{-1})[a]	Composition	Autoionizing rate (sec^{-1})
$2p^5 3s\,3p$	0	$0.98\,\vert\,^4S_{3/2}\rangle - 0.13\,\vert\,^4P_{3/2}\rangle$	4.13×10^5
	2841	$0.99\,\vert\,^4D_{7/2}\rangle$	0
	3187	$0.94\,\vert\,^4D_{5/2}\rangle - 0.21\,\vert\,^4P_{5/2}\rangle + 0.18\,\vert\,(^1P)^2D_{5/2}\rangle$	1.25×10^{10}
	3536	$-0.92\,\vert\,^4D_{3/2}\rangle + 0.23\,\vert\,^4P_{3/2}\rangle - 0.22\,\vert\,(^1P)^2D_{3/2}\rangle$	1.79×10^{10}
	3830	$-0.94\,\vert\,^4D_{1/2}\rangle + 0.22\,\vert\,(^1P)^2P_{1/2}\rangle + 0.20\,\vert\,^4P_{1/2}\rangle$	1.06×10^9
	4768	$0.91\,\vert\,^4P_{5/2}\rangle + 0.32\,\vert\,(^1P)^2D_{5/2}\rangle + 0.20\,\vert\,(^3P)^2D_{5/2}\rangle$	3.84×10^{10}
	5152	$0.76\,\vert\,^4P_{3/2}\rangle + 0.48\,\vert\,(^1P)^2D_{3/2}\rangle + 0.30\,\vert\,(^3P)^2D_{3/2}\rangle + 0.22\,\vert\,(^1P)^2P_{3/2}\rangle$	8.59×10^{10}
$2p^5 3s\,4s$	22 555	$-1.0\,\vert\,^4P_{5/2}\rangle$	2.93×10^{-3}
$2p^5 3s\,3d$	28 474	$0.97\,\vert\,^4P_{1/2}\rangle - 0.24\,\vert\,^4D_{1/2}\rangle$	2.02×10^6
	28 543	$0.86\,\vert\,^4P_{3/2}\rangle - 0.49\,\vert\,^4D_{3/2}\rangle$	1.76×10^8
	28 595	$-1.0\,\vert\,^4F_{9/2}\rangle$	0
	28 654	$0.72\,\vert\,^4D_{5/2}\rangle - 0.60\,\vert\,^4P_{5/2}\rangle - 0.33\,\vert\,^4F_{5/2}\rangle$	1.02×10^6
	28 703	$0.71\,\vert\,^4F_{7/2}\rangle - 0.70\,\vert\,^4D_{7/2}\rangle$	1.76×10^8
	29 168	$-0.73\,\vert\,^4F_{5/2}\rangle + 0.58\,\vert\,^4P_{5/2}\rangle + 0.26\,\vert\,(^1P)^2D_{5/2}\rangle$	5.08×10^9
	29 264	$-0.65\,\vert\,^4D_{3/2}\rangle + 0.54\,\vert\,^4F_{3/2}\rangle - 0.42\,\vert\,^4P_{3/2}\rangle + 0.22\,\vert\,(^1P)^2P_{3/2}\rangle - 0.21\,\vert\,(^1P)^2D_{3/2}\rangle$	1.55×10^9

[a] $\pm 2\ cm^{-1}$.

the radiative and autoionizing rates of $(2p^5 3s\,3p)^4S_{3/2}$ change only slightly to $9.6\times10^6\ sec^{-1}$ and $4.1\times10^5\ sec^{-1}$, respectively.

The next lowest level in the quartet manifold is $(2p^5 3s\,3p)^4D_{7/2}$, which has the largest J in its configuration. Neglecting configuration interaction, this level has a Coulombic autoionizing rate of zero. The levels $(2p^5 3s\,3p)^4S_{3/2}$ and $(2p^5 3s\,3p)^4D_{7/2}$ are the primary storage levels for the fluorescence enhancement experiments which are described in the following section.

Table I gives the calculated multiconfigurational composition and autoionizing rates for each of the levels discussed in the paper. Details of the RCN/RGN calculations are given in the Appendix. The energies are the experimental values which are obtained in the present work.

III. EXPERIMENTAL STUDIES

A. Hollow-cathode discharge

Population in core-excited levels of Na was produced by electron excitation in a pulsed hollow-cathode discharge.[13,14] Figure 1 shows the hollow-cathode design. The hollow cylindrical cathode, 30 cm long and 1.91 cm in diameter, is suspended inside the 2.09-cm-diam anode tube by three support rods, which also serve as the electrical connection to the cathode. All parts are made of type 304 stainless steel. We have experimented with various cathode lengths and have found that a spatially uniform-pulsed glow discharge can be produced in cathodes whose length-to-diameter aspect ratio is no larger than 3 to 5. For this reason we placed four 1-cm-diam holes evenly along the length of the 30-cm-long cathode, thereby effectively segmenting it into five shorter cathodes.

Attached to the ~90-cm-long anode tube are three sidearms. Together with the anode they form the cell body which contains the Na metal vapor. The three cathode support rods enter the anode interior through these sidearms. Machinable glass (Macor) insulators and *O*-ring seals center the support rods and maintain a vacuum seal. The central 50 cm length of the cell is heated by external nichrome heaters surrounding the anode and sidearm structure and by individual heating coils located inside the cathode support rods.

The cell operates as a heat pipe[15] with the hot Na vapor confined to the central region. Helium buffer gas, which is introduced at the ends of the anode and sidearms, prevents Na vapor from coating the anode end windows and sidearm insulators. The inner walls of the anode and sidearms are lined with several layers of fine-mesh stainless steel screen to promote recirculation of the liquid Na.

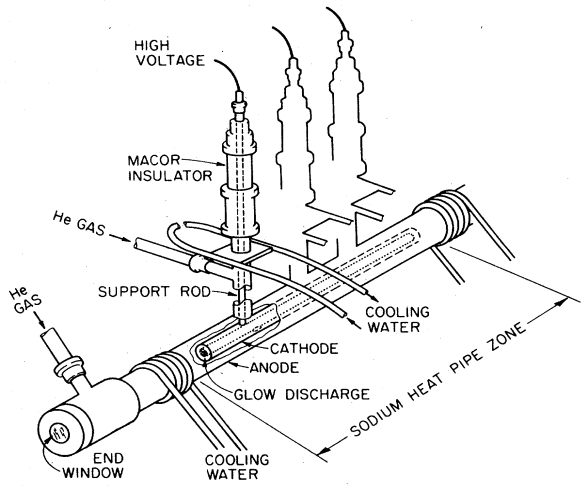

FIG. 1. Schematic diagram of the pulsed hollow-cathode discharge.

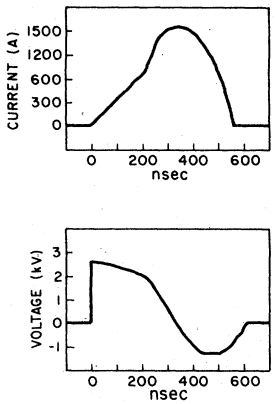

FIG. 2. Cathode-to-anode voltage and current characteristics of the hollow-cathode discharge.

Water-cooling rings keep the insulators and window flanges at room temperature when the central cell region is operated at ~ 550 °C. At these temperatures, absorption measurements of the $3s \rightarrow 4p$ transition at 3303 Å indicate a Na vapor pressure approximately equal to the He buffer-gas pressure, i.e., typically 4—8 Torr, or (5—10) $\times 10^{16}$ Na atoms/cm^3.

A simple *RC* circuit was used to supply high-voltage pulses to the cathode through the low-inductance support-rod—sidearm assembly. The discharge was pulsed at 10—100 Hz by using a thyratron switch (EG&G HY-32) to connect a charged 200 nF storage capacitor, charged to several kV, across the cathode and anode. Current and voltage waveforms are shown in Fig. 2. In contrast to the discharge behavior observed in Li,[13] the pulsed Na glow discharge degraded into an arc about 200 nsec after breakdown, at currents slightly in excess of 650 A. Fluorescence from excited ion levels and from neutral quartets (e.g., 3882 Å) decreased immediately after the arc commenced. Consequently, the emission experiments we describe were performed within a 50 nsec period immediately prior to the discharge arc.

The discharge could be run reliably for 50—100 h of operation. After this time the peak current would steadily decrease. Satisfactory operation could be restored by periodically cleaning and polishing the cathode and support-rod surfaces.

B. Na emission studies

Using the pulsed hollow-cathode discharge source, emission spectra of Na were recorded over the spectral region of 2500—6500 Å. The output from a 1-m Spex spectrometer (1200 lines/mm grating with 50-μm slits) was detected using an RCA C31034 photomultiplier tube. A boxcar integrator (Stanford Research Systems 250) averaged the pulsed fluorescence signals, which were recorded on a strip-chart recorder. Known Na I and Na II lines[16] provided calibration points in both first and second orders (e.g., the Na II line at 2842 Å was also used to calibrate the spectrum near 5684 Å). Both spectrometer and chart recorder were driven linearly in time by line-synchronous motors, thus allowing accurate linear interpolation between calibration wavelengths. The wavelengths reported here were measured to an accuracy of ± 0.2 Å.

The emission spectra were analyzed by tabulating the wavelengths and radiative intensities of unidentified lines. To discriminate against fluorescence from sputtered cathode elements and He emission lines, comparisons were made with spectra recorded in a cold hollow-cathode discharge. Of the remaining ~ 120 unidentified Na lines, the weakest was approximately 200 times less intense than the bright quartet line at 3881.8 Å (reported in Ref. 10 at 3882.8$\pm$2.0 Å). By comparing the relative intensities and positions of emission lines predicted by calculation to those observed experimentally, tentative identifications of some of the transitions were made.

C. Metastable population measurements

Among the tentative identifications was $(2p^5 3s\,3p)^4S_{3/2} \rightarrow (2p^5 3s\,4s)^4P_{5/2}$ at an observed wavelength of 4432.3 Å. This assignment was based upon calculated fine-structure splittings which placed $(2p^5 3s\,4s)^4P_{5/2}$ relative to the observed positions of $(2p^5 3s\,4s)^4P_{1/2,3/2}$ reported by Weiss,[17] and the observation in our laboratory[9] of the xuv decay of $(2p^5 3s\,3p)^4S_{3/2}$ to $(2p^6 3p)^2P$ at 405.26 Å. Together these level placements predicted the $^4S_{3/2}$-$^4P_{5/2}$ line at 4425$\pm$20 Å. The emission at 4432.3 Å was the only line near the expected wavelength.

Subsequently we observed absorption of a tunable laser probe beam at 4432.3 Å. By using the curve-of-growth technique,[18] the $(2p^5 3s\,3p)^4S_{3/2}$ population was estimated to be 2×10^{10} atoms/cm^3. For this measurement we used a calculated absorption oscillator strength of $f=0.06$, a Doppler width of 0.09 cm^{-1}, and a collision-broadened Lorentz width of 0.01 cm^{-1}. The population is comparable to that of the pure metastable $(2p^5 3s\,3p)^4D_{7/2}$ which we measure[14] at $\sim 10^{11}$ atoms/cm^3.

D. Laser-enhanced fluorescence

In these experiments the populations stored in the metastable Na quartets $(2p^5 3s\,3p)^4D_{7/2}$ and $(2p^5 3s\,3p)^4S_{3/2}$ were transferred to an upper level suggested by the RCN/RCG calculations and the emission spectra. Observation of the resulting fluorescence either confirmed or, in some cases, denied the earlier tentative assignments.

An example of the laser-enhancement technique is indicated schematically in Fig. 3. A Quanta-Ray pulsed dye

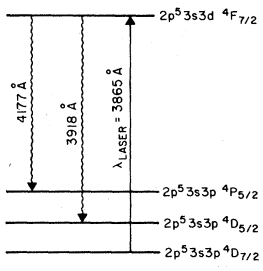

FIG. 3. Example of laser-induced fluorescence within the Na I quartet manifold. Population stored in the metastable level $(2p^5 3s\,3p)^4D_{7/2}$ is transferred by a laser at 3865 Å to $(2p^5 3s\,3d)^4F_{7/2}$ resulting in enhanced fluorescence at 3918 and 4177 Å.

laser was tuned through the predicted $(2p^5 3s\,3p)^4D_{7/2} \rightarrow (2p^5 3s\,3d)^4F_{7/2}$ transition at 3865.5 Å, thereby transferring stored population from the metastable $^4D_{7/2}$ level to the $^4F_{7/2}$ level. During the time the transfer laser was on, the intensities of all lines which may originate from this upper level were observed (e.g., 3918 Å). Those whose intensity increased (usually by a factor of 2–4) above the normal discharge intensity were taken to be correctly assigned. A check was made to see that lines that were not assigned this upper level were not enhanced.

Because the storage levels used in these experiments have total angular momentum $J=\frac{3}{2}$ and $\frac{7}{2}$, it was possible to transfer population via allowed dipole transitions to all possible J values ($\frac{1}{2}$–$\frac{9}{2}$) of the $2p^5 3s\,3d$ and $2p^5 3s\,4s$ configurations. The transfer laser power was ~20 kW/cm^2, which was sufficient to saturate all but the weakest ($f=10^{-4}$) transition, $(2p^5 3s\,3p)^4D_{7/2} \rightarrow (2p^5 3s\,3d)^4F_{5/2}$.

Experimentally the transfer laser was introduced into the discharge through a 1-cm^2 hole in the turning mirror used to direct the discharge fluorescence to the spectrometer. The intensity of a given line was monitored by the spectrometer as the dye laser was tuned through the transfer frequency. Output from the spectrometer photomultiplier tube was averaged by the boxcar integrator whose 20 nsec gate coincided with the laser pulse.

IV. RESULTS

The results of this study are summarized in Tables I and II and Fig. 4. In Table I we list the observed Na I quartet levels, in order of increasing energy relative to the lowest quartet, $(2p^5 3s\,3p)^4S_{3/2}$. The energies shown in

TABLE II. Na I quartet transition wavelengths, transition probabilities, branching ratios ($\mathscr{R}$), and observed line intensities.

Upper level	Lower level	λ (Å)[a]	A_{ik}(10^8 sec^{-1})	$g_i\mathscr{R}$	Experimental intensity[b]
$(2p^5 3s\,3d)^4P_{1/2}$	$(2p^5 3s\,3p)^4S_{3/2}$	3511.0	1.15	1.3	1.3
	$^4P_{3/2}$	4286.7	0.28	0.32	0.46
	$^4D_{3/2}$	4008.8	0.15	0.18	0.27
$^4P_{3/2}$	$^4S_{3/2}$	3502.5	0.88	1.0	1.6
	$^4P_{3/2}$	4273.9	0.16	0.18	0.23
	$^4P_{5/2}$	4204.9	0.25	0.28	0.46
	$^4D_{3/2}$	3997.7	0.08	0.09	0.14
	$^4D_{5/2}$	3942.6	0.21	0.24	0.32
$^4D_{3/2}$	$^4S_{3/2}$	3416.2	0.15	0.03	[c]
	$^4D_{1/2}$	3930.6	0.25	0.05	0.15
	$^4D_{3/2}$	3885.7	0.62	0.12	0.36
$^4D_{5/2}$	$^4S_{3/2}$	3489.0	0.42	1.5	1.3
	$^4P_{3/2}$	4253.8	0.05	0.18	0.17
	$^4P_{5/2}$	4185.5	0.49	1.8	1.5
	$^4D_{3/2}$	3980.3	0.05	0.18	0.14
	$^4D_{5/2}$	3925.6	0.45	1.6	0.85
	$^4D_{7/2}$	3872.9	0.12	0.45	0.19
$^4F_{5/2}$	$^4S_{3/2}$	3427.3	0.28	0.11	0.09
	$^4D_{5/2}$	3848.0	0.28	0.03	0.05
	$^4D_{3/2}$	3900.4	0.77	0.08	0.15
$^4F_{7/2}$	$^4P_{5/2}$	4176.7	0.35	0.83	0.82
	$^4D_{5/2}$	3917.9	0.66	1.5	1.6
	$^4D_{7/2}$	3865.5	0.58	1.4	1.3
$^4F_{9/2}$	$^4D_{7/2}$	3881.8	1.63[d]	10.0	4.2
$(2p^5 3s\,4s)^4P_{5/2}$	$^4S_{3/2}$	4432.3	0.14	0.91	3.1
	$^4P_{3/2}$	5744.2	0.04	0.23	0.12
	$^4P_{5/2}$	5621.0	0.14	0.91	0.42
	$^4D_{3/2}$	5256.4	0.02	0.16	0.07
	$^4D_{5/2}$	5162.5	0.15	1.0	0.83
	$^4D_{7/2}$	5071.2	0.41	2.7	2.7

[a]Air wavelengths, ±0.2 Å.
[b]Arbitrary units.
[c]Not observed in emission scans; transition observed in laser transfer $(2p^5 3s\,3p)^4S_{3/2} \rightarrow (2p^5 3s\,3d)^4D_{3/2}$.
[d]Ref. 10 reports $(1.32\pm0.2)\times10^8$ sec^{-1} (experimental) and 1.67×10^8 sec^{-1} (calculation by Weiss).

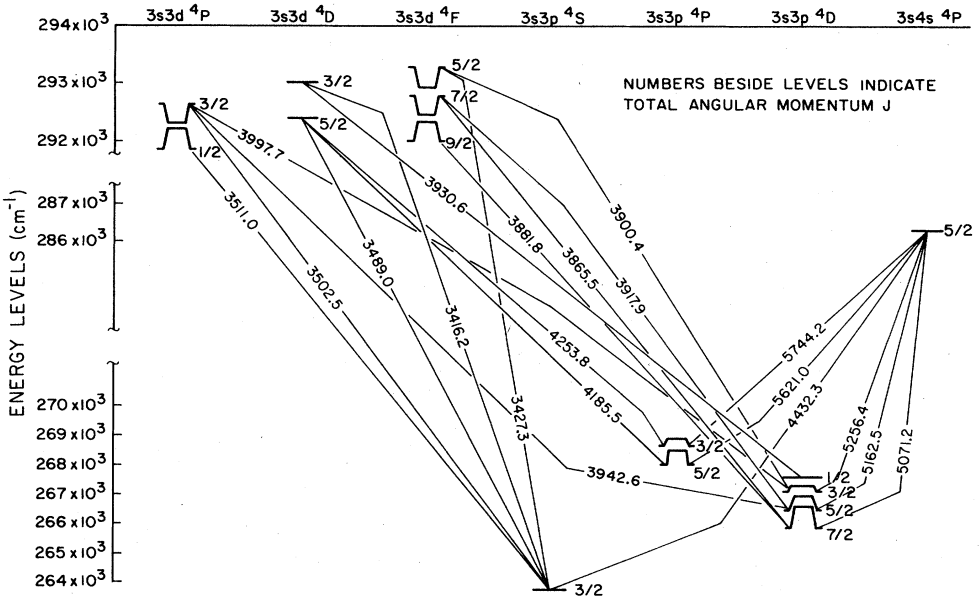

FIG. 4. Na I core-excited Grotrian diagram.

the first column are accurate to ± 2 cm^{-1}. Based upon the photoabsorption measurements of Sugar *et al.*,[6] which place $(2p^5 3s\,3p)^4P_{1/2}$ and $^4P_{3/2}$ relative to the Na ground level, the energy of $(2p^5 3s\,3p)^4S_{3/2}$ is 263773 ± 15 cm^{-1}. The calculated *LS*-basis eigenvectors of the observed levels are shown in the second column of Table I. Components present in excess of 4% are listed. (Components mixed in by configuration interaction were less than 0.7%.) The third column gives the calculated Coulombic autoionizing rates. Details of these calculations are given in the Appendix.

Table II lists the observed Na I quartet-quartet transition wavelengths, grouped in series characterized by a common upper level. We have labeled levels by giving the largest *LS*-coupled component. All identifications listed in this table were verified by laser-enhanced fluorescence. That is, each upper level was populated by laser transfer of stored population from the metastable levels $(2p^5 3s\,3p)^4S_{3/2}$ or $^4D_{7/2}$, as allowed by the electric dipole selection rule $\Delta J = 0, \pm 1$, and enhanced fluorescence was observed consistent with the assignments in Table II. [Transfer to the $(2p^5 3s\,3d)^4F_{5/2}$ level from $(2p^5 3s\,3p)^4D_{7/2}$, although allowed by selection rules, was not attempted because the required transfer power (200 kW/cm^2) was not available. Instead, the transfer experiment $(2p^5 3s\,3p)^4S_{3/2}$ to $(2p^5 3s\,3d)^4F_{5/2}$ was performed.] In each transfer experiment the laser wavelength (calibrated to ± 0.3 Å) at which the fluorescence enhancement was maximum agreed with the discharge fluorescence wavelength measured previously with the spectrometer (± 0.2 Å).

Table II also gives the calculated Einstein A coefficient and branching ratio ($\mathscr{R}$). The latter is defined for the transition from the upper level i to the lower level j as

$$\mathscr{R} = \frac{A_{ij}}{\sum_k A_{ik} + W_i^{\mathrm{AI}}},$$

where A_{ik} is the spontaneous radiative rate to a lower level k and W_i^{AI} is the calculated autoionizing rate of the upper level i.

The last column of Table II gives the relative intensities of each of the lines as observed in the emission spectra (i.e., unenhanced intensities). Lines from the $2p^5 3s\,3d$ and $2p^5 3s\,4s$ upper levels have been normalized separately, since the cross sections for electron excitation of these two configurations are not the same. Intensities have also been adjusted to account for the wavelength response of the spectrometer grating and photomultiplier tube.

The rapid radiative and autoionizing rates probably exceed collisional deexcitation rates in the hollow-cathode discharge. Under these conditions the fluorescence line intensities from upper levels of the same configuration should be proportional to $g_i\mathscr{R}$, where g_i is the upper level degeneracy. To compare with experiment, the observed intensities from $2p^5 3s\,3d$ upper levels were normalized such that the intensity of 3511 Å $[(2p^5 3s\,3d)^4P_{1/2} \rightarrow (2p^5 3s\,3p)^4S_{3/2}]$, measured in arbitrary units, was equal to the calculated quantity $g_i\mathscr{R}$ for that transition. Similarly, all observed intensities from $(2p^5 3s\,4s)^4P_{5/2}$ were normalized such that the 5071 Å $[(2p^5 3s\,4s)^4P_{5/2}$

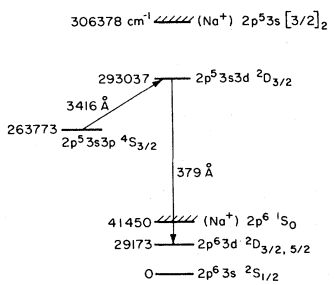

FIG. 5. Energy-level diagram for a 379 Å laser in Na.

TABLE III. xuv lasers in Na I.

Laser upper level	$(2p^5 3s\,3d)^4D_{3/2}$	$(2p^5 3s\,3d)^4F_{5/2}$	$(2p^5 3s\,3d)^2D_{5/2}$
Laser wavelength	378.98 Å	379.12 Å	375.3 Å
gf_{laser}	0.038	0.055	0.485
σ_{gain} (cm^2)	6.9×10^{-15}	6.5×10^{-15}	5.6×10^{-14}
τ_{AI} (Laser upper level)	645 psec	196 psec	45 psec
gf_{transfer}	0.10	0.30	0.011
$\lambda_{\text{transfer}}$	3416 Å	3427 Å	≈3140 Å

$\rightarrow(2p^5 3s\,3p)^4D_{7/2}]$ intensity equaled the corresponding $g_i\mathscr{R}$. Normalization using these two wavelengths was found to give good overall fit of observed intensities to calculated branching ratios for all of the transitions of Table II. Observed line intensities were found to agree to within a factor of 3.5 with the predicted intensities. A Grotrian diagram showing many of the brighter transitions is given in Fig. 4.

It is of interest to note that fluorescence enhancement of all lines of Table I was observed when the transfer laser was tuned to the Na II transition $2p^5 3s[\frac{3}{2}]_2 \rightarrow 2p^5 3p[\frac{1}{2}]_1$ at 3533 Å. We measure a metastable ion population in $2p^5 3s[\frac{3}{2}]_2$ of 5×10^{12} ions/cm^3. Transferring this population to $2p^5 3p[\frac{1}{2}]_1$ allows exothermic spin exchange and charge transfer to quartet levels in the $2p^5 3s\,3d$ and $2p^5 3s\,4s$ neutral configurations. Enhancements of 7—10 times the background intensities noted in Table II were typically observed. This may suggest a useful method of identifying emission lines that emanate from core-excited levels.

V. SODIUM 379 Å LASER

Based on the spectroscopy reported here, several xuv lasers of the store-transfer type proposed by Harris are well defined.[1,2] Figure 5 shows a 379 Å laser in which population stored in the quasimetastable level $(2p^5 3s\,3p)^4S_{3/2}$ is transferred to the upper laser level $(2p^5 3s\,3d)^4D_{3/2}$. The latter has a calculated spontaneous decay rate (due to mixing with doublets of the same configuration) of 4.4×10^8 sec^{-1} for radiating to the lower laser level $(2p^6 3d)^2D$. At a Doppler width of 1.13 cm^{-1} (about 10 Torr of Na vapor pressure), the gain cross section at 379 Å is 6.9×10^{-15} cm^2. The oscillator strength for the transfer laser at $\lambda=3416$ Å is $f=0.025$, which for the calculated 645 psec autoionizing lifetime of the upper level corresponds to a per atom saturating power density of ~5 kW/cm^2.

Table III summarizes the parameters of three possible xuv lasers in neutral Na. All three are based on population storage in the level $(2p^5 3s\,3p)^4S_{3/2}$. The first two make use of levels which are defined in this study, but have a somewhat smaller xuv-gain cross section than does the third. This latter case ($\lambda=375$ Å) has an upper level which is dominantly of doublet character. However, we have been unable to observe it in visible emission and, based on xuv studies, its energy remains uncertain to about 70 cm^{-1}. The lower level for the xuv transition in all three cases is $(2p^6 3d)^2D$.

VI. SUMMARY

The work described here demonstrates the use of a pulsed hollow-cathode discharge to obtain metastable atom densities of about 10^{11} atoms/cm^3 in low-lying quartet levels of neutral Na. Laser-enhanced fluorescence, produced by population stored in these levels, together with RCN/RCG Hartree-Fock calculations, establish the identity and energy of 15 quartet levels within the quartet manifold. Twenty-eight newly identified transitions between these levels are reported. Several possible xuv laser systems are described.

ACKNOWLEDGMENTS

The work described here was supported by the U.S. Air Force Office of Scientific Research and the U.S. Army Research Office and the National Science Foundation. The authors wish to acknowledge the contributions to this work made by R. W. Falcone and J. F. Young. We also acknowledge many helpful discussions with R. G. Caro, R. D. Cowan, T. B. Lucatorto, A. J. Mendelsohn, K. D. Pedrotti, A. W. Weiss, and P. J. K. Wisoff.

APPENDIX

The Coulombic autoionization and dipole radiative rates of Na I core-excited levels used in this study were calculated using the atomic-physics codes RCN/RCG.[3]

TABLE IV. Configuration-average energies for RCN/RCG calculations.

Configuration	E_{average} (cm^{-1})
$2p^6 3s$	0
$2p^6 4s$	25 849
$2p^6 3d$	29 267
$2p^6 4d$	33 676
$2p^5 3s^2$	251 768
$2p^5 3s\,3p$	271 994
$2p^5 3s\,4s$	287 318
$2p^5 3s\,3d$	293 060
$2p^5 3s\,4p$	293 791
$2p^5 3s\,4d$	299 865
$2p^5 3p^2$	302 380
$2p^5 3s\,5d$	303 711
$2p^5 3p\,4s$	319 540
$2p^5 3p\,3d$	324 008

TABLE V. Radial integral scaling factors used to adjust HF values. The same scaling factors were used for all of the configurations.

Hartree-Fock integral	Scaling factor
$F^k(i,i)$	0.82
$F^k(i,j)$	0.82
$G^k(i,j)$	0.72
$R^k(i,j)$	0.77
ζ_i	1.00

These calculations included the even-parity configurations $2p^5 3s\,3p$, $2p^5 3s\,4p$, $2p^5 3p\,4s$, $2p^5 3p\,3d$, and continuum configurations $2.03s$, $2.03d$, $2.23s$, $2.23d$, where the notation $2.03l$ indicates a continuum electron with an energy of 2.03 Ry and orbital angular momentum l. The odd-parity configurations included were $2p^5 3s\,3d$, $2p^5 3s\,4d$, $2p^5 3s\,5d$, $2p^5 3s^2$, $2p^5 3p^2$, $2p^5 3s\,4s$, $2.22p$, $2.22f$, $2.32p$, and $2.32f$. The configuration-average energies and radial integrals were adjusted to give reasonable agreement with the level energies of Refs. 5—7. In particular, the $(2p^5 3s\,3p)^4D_{7/2} \rightarrow (2p^5 3s\,3d)^4F_{9/2}$ transition wavelength was placed at 3882 Å. The configuration-average energies and radial integral scaling factors used are listed in Tables IV and V.

The RCN/RCG oscillator strength of the 3882-Å transition agrees to within a factor of 1.25 with the experimental value.[10] Because of the good agreement between predicted and observed quartet line intensities, we estimate that the quartet radiative transition rates in Table II and autoionizing rates of Table I are accurate to within factors of 2—4.

[1]S. E. Harris, Opt. Lett. **5**, 1 (1980).

[2]Joshua E. Rothenberg and Stephen E. Harris, IEEE J. Quantum Electron. **QE-17**, 418 (1981).

[3]Robert D. Cowan, *The Theory of Atomic Structure and Spectra* (University of California, Berkeley, 1981), Secs. 8-1, 16-1, and 18-7.

[4]P. Feldman and R. Novick, Phys. Rev. **160**, 143 (1967).

[5]H. W. Wolff, K. Radler, B. Sonntag, and R. Haensel, Z. Phys. **257**, 353 (1972); J. P. Connerade, W. R. S. Garton, and M. W. D. Mansfield, Astrophys. J. **165**, 203 (1971).

[6]J. Sugar, T. B. Lucatorto, T. J. McIlrath, and A. W. Weiss, Opt. Lett. **4**, 109 (1979).

[7]E. Breuckmann, B. Breuckmann, W. Mehlhorn, and W. Schmitz, J. Phys. B **10**, 3135 (1977); E. J. McGuire, Phys. Rev. A **14**, 1402 (1976); K. J. Ross, T. W. Ottley, V. Pejcev, and D. Rassi, J. Phys. B **9**, 3237 (1976); D. J. Pegg, H. H. Haselton, R. S. Thoe, P. M. Griffin, M. D. Brown, and I. A. Sellin, Phys. Rev. A **12**, 1330 (1975).

[8]Yu. V. Zhmenyak, V. S. Vukstich, and I. P. Zapesochnyi, Pis'ma Zh. Eksp. Theor. Fiz. **35**, 321 (1982) [JETP Lett. **35**, 393 (1982)].

[9]K. D. Pedrotti, A. J. Mendelsohn, R. W. Falcone, J. F. Young, and S. E. Harris (unpublished).

[10]H. G. Berry, R. Hallin, R. Sjödin, and M. Gaillard, Phys. Lett. **50A**, 191 (1974).

[11]R. Fröhling and H. J. Andrä, Phys. Lett. **97A**, 375 (1983).

[12]S. E. Harris, D. J. Walker, R. G. Caro, A. J. Mendelsohn, and R. D. Cowan, Opt. Lett. **9**, 168 (1984).

[13]R. W. Falcone and K. D. Pedrotti, Opt. Lett. **7**, 74 (1982).

[14]D. E. Holmgren, R. W. Falcone, D. J. Walker, and S. E. Harris, Opt. Lett. **9**, 85 (1984).

[15]C. R. Vidal and J. Cooper, J. Appl. Phys. **40**, 3370 (1969).

[16]A. R. Striganov and N. S. Sventitskii, *Tables of Spectral Lines of Neutral and Ionized Atoms* (IFI/Plenum, New York, 1968), pp. 231—235; *MIT Wavelength Tables* (MIT Press, Cambridge, Mass., 1982), pp. 380 and 381.

[17]A. W. Weiss (private communication).

[18]S. S. Penner and R. W. Kavanagh, J. Opt. Soc. Am. **43**, 385 (1953).